Modulator Mediated Functionalization (MoFu) of MOF-808 as a Platform Tool to Create High-Performance Mixed-Matrix Membranes

*Raymond Thür, Niels Van Velthoven, Vincent Lemmens, Maarten Bastin, Simon Smolders, Dirk De Vos, Ivo F.J. Vankelecom**

Centre for Membrane Separations, Adsorption, Catalysis and Spectroscopy for Sustainable Solutions (cMACS), KU Leuven, Celestijnenlaan 200F, Box 2454, 3001 Heverlee, Belgium

E-mail: ivo.vankelecom@kuleuven.be

Keywords: fluorinated MOF-808, platform MOF, modulator mediated functionalization, mixed-matrix membranes, CO_2/CH_4 separation

Abstract

Modulator mediated functionalization (MoFu) is introduced as a new and versatile platform tool to improve the separation performance of MOF-based membranes, exemplified here by the creation of mixed-matrix membranes (MMMs) with enhanced CO_2 separation efficiency. The unique structure of MOF-808 allows incorporation of CO_2-philic modulators in the MOF framework during a one-pot synthesis procedure in water, thus creating a straightforward way to functionalize both MOF and corresponding MMM. As a proof of concept, a series of fluorinated carboxylic acids (trifluoroacetic acid (TFA), pentafluoropropionic acid (PFPA) and heptafluorobutyric acid (HFBA)) and non-fluorinated alkyl carboxylic acids (acetic acid (AA), propionic acid (PA) and butyric acid (BA)) were used as modulator during MOF-808 synthesis. Two of the best MMMs prepared with 30 wt% MOF-TFA (100% increase in CO_2/CH_4 separation factor, 350% increase in CO_2 permeability) and 10 wt% MOF-PFPA (140% increase in CO_2/CH_4 separation factor, 100% increase in CO_2 permeability) scored very close to or even crossed the 2008 and 2018 upperbound limits for CO_2/CH_4. Due to its facile functionalization (and its subsequent excellent performance), MOF-808 is proposed as an alternative for widely used UiO-

66, which is, from a functionalization point-of-view and despite its widespread use, a rather limited MOF.

1 Introduction

As the effects of a global rise in temperature become clearer and more pronounced, efficient strategies for carbon capture are highly desired and topical. Membrane-based CO_2 separation is considered a green alternative for traditional carbon capture technologies (e.g. amine scrubbing, adsorption, cryogenic distillation) thanks to its relatively low energy footprint and easy retrofitting into existing plants.[1]

Combination of the advantages of organic polymers and inorganic fillers has been extensively studied as a means to create more efficient membranes, resulting in the development of mixed-matrix membranes (MMMs) for gas separation or liquid separations, such as reverse osmosis or solvent-resistant nanofiltration (SRNF). For both gas and liquid separations, the main target is to move the separation performance towards both high fluxes and high selectivities.[2] Especially for the separation of CO_2 from natural or biogas, a lot of effort has been dedicated to finding new polymer-filler combinations with enhanced separation performance.[3–8] In this context, metal-organic frameworks (MOFs) were proposed as a new filler material for MMM preparation about a decade ago.[7,9–15] MOFs are a class of crystalline fillers, consisting of metal nodes or clusters connected with organic linkers.[11] For example, UiO-66 (and its functionalized derivatives), consisting of hexanuclear $Zr_6O_4(OH)_4$ clusters connected by 12 1,4-benzenedicarboxylate (BDC^{2-}) linkers, is one of the most reported fillers in MMM literature to increase membrane permeability[16,17] as it has a good porosity and specific surface area and shows excellent thermal, chemical and mechanical stability, owing to the high coordination number of the Zr-oxo cluster.[18]

Although UiO-66 MMMs definitely have their respective advantages, one should expect from novel MMM materials to not only increase the membrane's permeability but also simultaneously the selectivity. In this sense, UiO-66 faces some serious limitations. As the cluster coordination sphere is theoretically fully occupied by BDC^{2-} linkers, few additional coordination sites are available for introducing functional ligands, besides a limited number of missing-linker defects.[20] Especially with regard to creating functionality inside the MOF framework (to enhance CO_2-philicity), a lot of progress can be realized compared to traditional functionalization methods (e.g. through linker functionalization or grafting) of UiO-66 and ZIF-8 (for example UiO-66-NH_2 or bipyridine-based UiO-67), which often entail the use of expensive organic linkers, in addition to potential negative consequences regarding porosity and surface area.[17,21]

Bearing this in mind, MOF-808 is here proposed as an alternative to UiO-66 for future MMM development. Almost a decade after the discovery of UiO-66, MOF-808 was first synthesized by the Yaghi group[22] and has been used in e.g. catalysis and gas detection.[23–26] Compared to UiO-66, MOF-808 exhibits a higher surface area and larger pore volume, but at the same time, equally excellent thermal, chemical and mechanical stability.[27] Both UiO-66 and MOF-808 are based on the same $Zr_6O_4(OH)_4$ clusters, respectively linked by ditopic BDC^{2-} and tritopic 1,3,5-benzenetricarboxylate (BTC^{3-}) linkers. Whereas the UiO-66 Zr-cluster is theoretically coordinatively saturated with 12 BDC^{2-} linkers, the coordination sites on the Zr-cluster in MOF-808 are occupied by only 6 linker carboxylate groups (three at opposing vertices of the cluster), leaving the 6 remaining equatorial sites available for coordination with modulators or other ligands (Figure 1).[20,27]

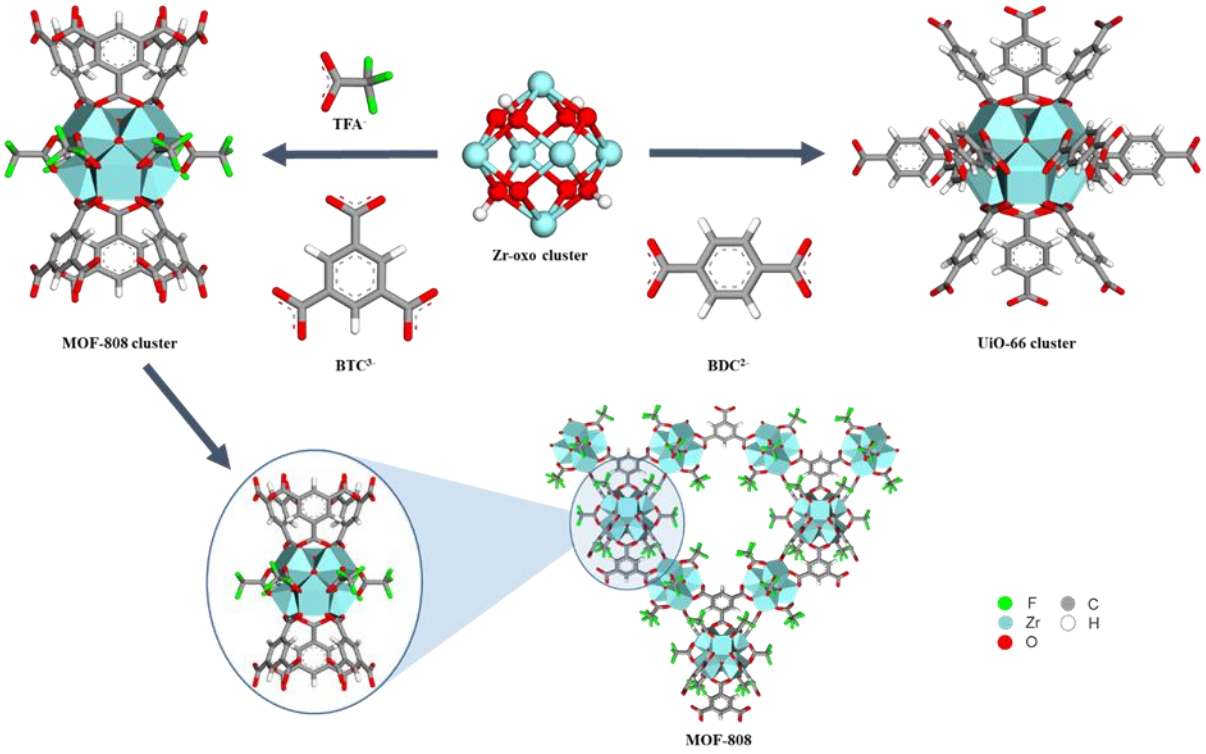

Figure 1: Comparison between TFA modulated MOF-808 cluster and UiO-66 cluster.

This unique feature allows for introducing functionalized moieties in the MOF framework by selecting a specific modulator (e.g. trifluoroacetic acid) without having to apply expensive and difficult-to-synthesize functionalized organic linkers.

In this work, MOF-808 is introduced as a new platform MOF for membrane-based CO_2 capture and as a versatile alternative for UiO-66. Advantages of MOF-808 entail (1) easy one-pot synthesis in water[28], (2) low cost components and facile upscaling[28], (3) large pore volume and specific surface area[22], and most importantly, (4) straightforward and cheap functionalization by modulation. To systematically illustrate the principle of functionalization by modulation, three alkyl carboxylic acids (acetic acid (AA), propionic acid (PA), butyric acid (BA)) and their fluorinated counterparts (trifluoroacetic acid (TFA), pentafluoropropionic acid (PFPA), heptafluorobutyric acid (HFBA)) were used as modulator during MOF synthesis. The resulting

MOFs were then incorporated in Matrimid membranes and tested for their use in membrane-based CO_2/CH_4 separation.

2 Experimental section

2.1 Chemicals

Polyimide (Matrimid 5218) was kindly provided by Huntsman (Switzerland). Tetrahydrofuran (THF, >99%) and N,N-dimethylformamide (DMF, >99%) were purchased from Acros. Ethanol (pure) was purchased from Fischer. CO_2 and CH_4 gases were purchased from Air Liquide (Belgium). AA, PA, BA, PFPA, HFBA were supplied by Sigma-Aldrich. TFA was purchased from Merck-Schuchardt while zirconylchloride octahydrate was supplied by Abcr GmbH. Benzene tricarboxylic acid was purchased from J&K Chemicals.

2.2 MOF synthesis

MOF-AA, MOF-PA, MOF-BA, MOF-TFA, MOF-PFPA and MOF-HFBA were synthesized following a recipe described in reference[28] but with variation of the modulator type. First, 0.605 mmol (0.127 g) BTC and 1.815 mmol (0.585 g) $ZrOCl_2.8H_2O$ were added to a 10 mL crimp cap vial. Subsequently, 4.55 mL demi-H_2O and 17.8 mmol modulator (being AA, PA, BA, TFA, PFPA or HFBA) were added. The mixture was then heated to 100 °C in a heating block with stirring for 24 h. Afterwards, the MOF sludge was washed with water (3 times) and with THF (3 times). After each washing step, the samples were centrifuged. The washed MOF was stored in THF until further use. Different particle sizes for MOF-TFA were obtained by adding different amounts of solvent during MOF synthesis: 4 mL H_2O for MOF-TFA-1300, 2 mL H_2O for MOF-TFA-550, 1 mL H_2O for MOF-TFA-150.

UiO-66 was prepared by adding 1.82 mmol (0.58g) $ZrOCl_2.8H_2O$, 1.82 mmol (0.30g) 1,4-benzenedicarboxylic acid, 5 mL water and 5 mL acetic acid to a 10 mL crimp cap vial. The mixture was then heated under stirring at 100 °C for 24 h. Afterwards, the MOF sludge was washed with

water (3 times) and with THF (3 times). After each washing step, the samples were centrifuged. The washed MOF was stored in THF until further use.

2.3 Membrane synthesis

Polymer membrane synthesis

0.42 g of polymer (Matrimid) was dissolved in THF (5.58 g). The polymer solution was then stirred overnight and poured by hand into a Teflon Petri dish (diameter 6 cm) under N_2 atmosphere at room temperature. A plastic funnel was placed on top to slow down the solvent evaporation rate. When the solid membrane film was formed, it was annealed in a muffle oven while following the temperature profile: heating to 110 °C at 5 °C/min, 2 h at 110 °C, heating to 180 °C at 5°C/min and 6 h at 180 °C.

Mixed-matrix membrane synthesis

Since a wet synthesis method was applied[29], the MOF quantity was determined by using a calibration curve. 1, 2 and 3 mL of the MOF in THF suspension were transferred with a pipette to glass beakers and dried overnight at 100 °C. The used volume of MOF suspension was then correlated with the actual MOF mass. Using the calibration curve, the desired amount of wet MOF (in THF) was determined and further diluted with 5.58 g THF. After stirring and sonication, 0.42 g polymer was added in three portions according to a priming protocol[21]. Before polymer addition, the polymer/MOF suspensions were sonicated for 30 min and continuously stirred. Prior to casting, the suspensions were again sonicated. Casting and annealing of the MMM films occurred according to the same procedure as for the unfilled membranes. Filler loading was determined with the following equation:

$$\text{filler loading (wt\%)} = 100 * \left(\frac{m_{filler}}{m_{filler} + m_{polymer}} \right) \quad \text{(Equation 1)}$$

2.4 Characterization

Powder X-ray diffraction patterns (XRD) of MOFs and membranes were recorded on a Malvern PANalytical Empyrean diffractometer in transmission mode over a 1.3-45° 2Θ range, using a PIXcel3D solid state detector and Cu anode (Cu Kα1: 1.5406 Å; Cu Kα2: 1.5444 Å).

Membrane cross-sections and MOF particle morphologies were studied with scanning electron microscopy (SEM, Philips XL30 FEG). Membrane cross-sections were prepared by breaking the membranes in liquid nitrogen and a gold/palladium coating was applied on all samples before measurement.

Thermogravimetric analysis (TGA, TA instruments TGA Q500) was performed to study the behavior of membranes and MOF when heated to high temperatures. Both membrane and MOF samples were heated in presence of O_2 at a heating rate of 5 °C/min.

A Varian 670 FTIR imaging microscope with a Single Point MCT detector and a diamond ATR crystal was used to perform attenuated total reflectance – Fourier transform infrared spectroscopy (ATR-FTIR) and to study chemical changes and functional groups in membranes and MOFs. Thirty-two scans were collected at a resolution of 4 cm^{-1}.

Differential scanning calorimetry (DSC, TA instruments DSC Q2000) experiments were conducted on the polymer membranes and MMMs. Membranes were first heated to 375 °C to erase the thermal history of the polymer. This was followed by the measurement cycle which comprised of cooling down to 275 °C and reheating to 375 °C. TA Universal Analysis was used for data analysis.

Density measurements were carried out on all membranes. The buoyancy method was applied to determine the experimental density with help of a Sartorius YDK 01 Density Determination Kit. Water was selected as the buoyancy liquid. The weight of the membrane sample was first measured in air and then in water. The resulting values were used in Equation 2:

$$\rho = \frac{W(a)}{0.99983}\left[\frac{\rho(fl)-0.0012\ g/cm^3}{W(a)-W(fl)}\right] + 0.0012\ g/cm^3 \qquad \text{(Equation 2)}$$

with W(a) and W(fl), the weight of the sample in air and water, respectively. Density of water, ρ(fl), is taken to be 0.99821 g/cm^3 at 20.1 °C while density of air is 0.0012 g/cm^3. 0.99983 is a correction factor for buoyancy of the set-up wires.

A Micromeritics 3Flex surface analyzer was used for gas sorption experiments. Experiments were conducted at -196 °C (liquid N_2). Before measuring, all MOFs were activated under vacuum at 100 °C for 16 h. Surface areas were calculated via the multi-point BET method applied to the isotherm adsorption branch, taking into account surface area criteria as given by Rouquerol[30] and the consistency criteria described by Walton and Snurr[31].

^{1}H and ^{19}F liquid phase nuclear magnetic resonance (NMR) were performed on MOF samples. For ^{1}H NMR, 600 µL deuterated dimethylsulfoxide was used to dissolve 3 mg MOF-808 by addition of 40 µL of a 40 wt.% hydrofluoric acid solution. The samples for ^{19}F NMR were prepared in a similar way with the addition of 10 µL fluorobenzene as internal standard. A recycle delay time (d1) of 30 s was used. The spectra were recorded on a Bruker AMX-300 spectrometer at 300 MHz (16 scans) and analyzed using SpinWorks 4.2 software.

Membrane performance characteristics (permeability and separation factor) were determined in our in-house developed High-Throughput Gas Separation (HTGS) set-up.[32,33] Simultaneous

measurement of 16 membranes can be performed in HTGS at different temperatures and pressures. Membrane coupons had a permeation area of 1.91 cm^2.

A constant-volume varying-pressure method was used to measure gas permeability. The membrane permeate was accumulated in an auxiliary cylinder of 75 cm^3. A vacuum sensor was used to measure the increase in pressure as a function of time (dp/dt). Gas permeability (P) of the membrane was then calculated via:

$$P_{CH4}=10^{10}\ \frac{y_{CH4}\times V\times L}{x_{CH4}\times P_{up}\times A\times R\times T}\ \frac{dp}{dt} \qquad \text{(Equation 3)}$$

$$P_{CO2}=10^{10}\ \frac{y_{CO2}\times V\times L}{x_{CO2}\times P_{up}\times A\times R\times T}\ \frac{dp}{dt} \qquad \text{(Equation 4)}$$

with y_i the mole fraction of the component in the permeate, x_i the mole fraction of the component in the feed, V the downstream volume (cm^3), A the membrane permeation area (1.91 cm^2), L the membrane thickness (cm), T the operating temperature (K), Pup the upstream pressure (cmHg), R the gas constant and dp/dt the pressure increase (cmHg/s).

Mixed-gas separation factors were determined as the ratio of the downstream (y) and upstream (x) mole fraction of the two gases by the following equation:

$$\alpha_{CO2/CH4}=\ \frac{y_{CO2}/y_{CH4}}{x_{CO2}/x_{CH4}} \qquad \text{(Equation 5)}$$

with y_{CO2} and y_{CH4} the mole fractions of CO_2 and CH_4 in the permeate, x_{CO2} and x_{CH4} the mole fractions of CO_2 and CH_4 in the feed. During gas chromatography analysis, y_{CO2}/y_{CH4} is determined from peak areas linked to mole fractions in the permeate, while x_{CO2}/x_{CH4} is determined by the feed settings.

3 Results and discussion

3.1 Modulator mediated functionalization: fluorinated MOF-808

Characterization of MOFs and membranes

As mentioned before, the unsaturated coordination sphere of the Zr-oxo cluster of MOF-808 allows for introduction of functionalized modulator molecules. In this way, modulation of MOF-808 can be used as a versatile approach towards creating MOFs with a high CO_2 preference over other gases such as N_2 and CH_4. With this concept of "modulator mediated functionalization" (MoFu) in mind and knowing that CO_2 shows excellent quadrupole-dipole interaction with polarized C-F bonds, TFA modulated MOF-808 samples with different particle sizes (ranging on average from 150 nm to 1.3 μm) were synthesized and incorporated in Matrimid membranes. The different MOF samples are denoted as MOF-TFA-*x* and the corresponding Matrimid MMMs as Matrimid-TFA-*x*, with *x* being the average particle size in nm.

XRD data show that highly crystalline MOF-808 particles can be made by using TFA as modulator and that there is a good agreement with the simulated XRD pattern of MOF-808 (Figure 2 and Figure S1-4). Furthermore, ATR-FTIR confirmed the appearance of an intense doublet signal at ~1170 and ~1205 cm^{-1}, indicating the presence of symmetrical and anti-symmetrical C-F stretching vibrations.[34]

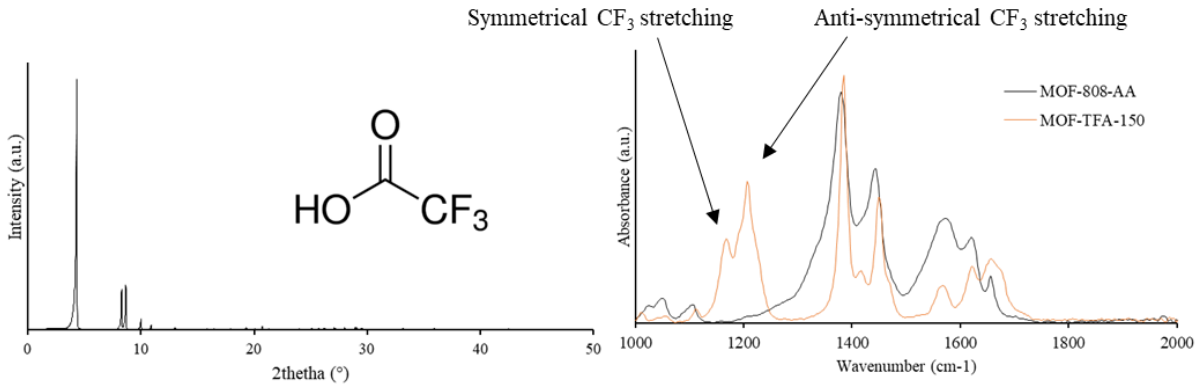

Figure 2: XRD pattern (left) and ATR-FTIR spectrum (right) of MOF-TFA-150. The IR spectrum for MOF-TFA-150 is compared to that of AA modulated MOF-808 (MOF-808-AA).

Octahedral MOF crystals were successfully synthesized with particle sizes ranging from 150 to 1300 nm (Figure 3). Visual analysis of the SEM images of the different sized MOFs with ImageJ gave size distribution plots given in Figure S11-13. Relatively homogeneous size distributions were obtained for MOF-TFA-150 and MOF-TFA-550 while synthesis of MOF-TFA-1300 was found to result in particles with a higher polydispersity. For the 150 nm and 550 nm particles, low solvent concentrations caused a highly concentrated synthesis mixture, which quickly formed a homogeneous gel.[35] This hinders the supply of fresh reactants to the MOF nuclei, slowing down the crystal growth rate relative to the nucleation rate and resulting in small, homogeneous particles. In more diluted reaction mixtures such as those used for MOF-TFA-1300, reactant diffusion was not hampered and the crystal growth rate overcame the nucleation rate.[36] Furthermore, N_2 physisorption showed a decreased Brunauer-Emmett-Teller (BET) surface area upon switching the modulator from AA to TFA (Table 1 and Figure S16). Despite the significantly lower surface area, the TFA modulated MOF exhibited an almost equal CO_2 uptake to that of MOF-AA (Figure S17). When normalized for the BET surface area, the CO_2 uptake was found to be 50% higher than that of MOF-AA. In addition, the sleeper initial slope of the CO_2 sorption isotherm confirms that the use of fluorinated modulator enhances the CO_2 affinity of the MOF.

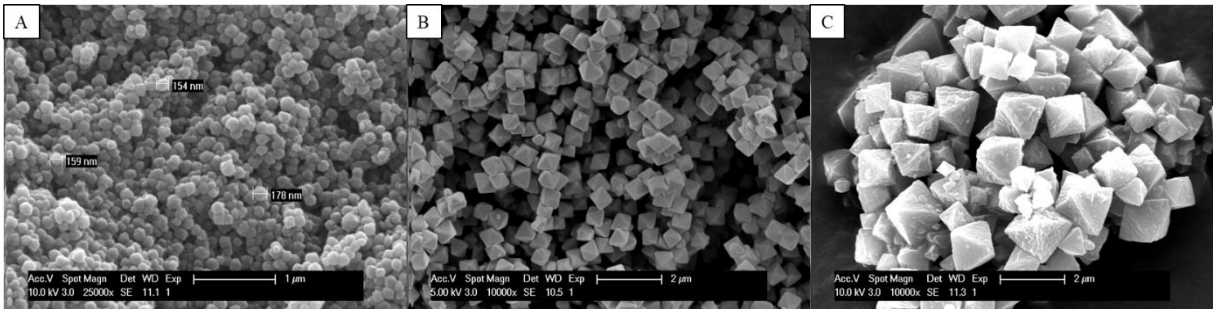

Figure 3: SEM images of (A) MOF-TFA-150, (B) MOF-TFA-550 and (C) MOF-TFA-1300.

After MOF synthesis, MMMs with different sized MOFs were prepared. Thermal stability of the MMMs was studied with TGA (Table S1 and Figure S18) while DSC was used to determine the glass transition temperature (T_g) of the pure polymer membrane and the MMMs (Table S1). Table S1 shows a high thermal stability for all membranes in the same range as that of the unfilled membrane. A slight decrease in thermal stability can be observed for MMMs with increasing particle size. DSC shows an increase in T_g for all MMMs compared to pristine Matrimid after incorporation of 10 wt% MOF, which can be explained by reduced polymer chain mobility due to presence of the MOF particles and thus a certain extent of polymer rigidification.[37]

Table 1: Comparison of MOF-AA and MOF-TFA-550 with regard to BET surface area, pore volume and CO_2 uptake.

	BET surface area (m^2/g)	**Pore volume (cm^3/g)**	**CO_2 uptake (cm^3/g)**
MOF-AA	1982	0.65	49.2
MOF-TFA	1239	0.49	46.0

Furthermore, SEM cross-sections (Figure 4 and Figure S6-8) suggest a good incorporation of the particles without evidence for sieve-in-a-cage morphology or severe particle clustering. Matrimid-TFA-1300 shows a less uniform incorporation of the fillers, probably due to size effects.

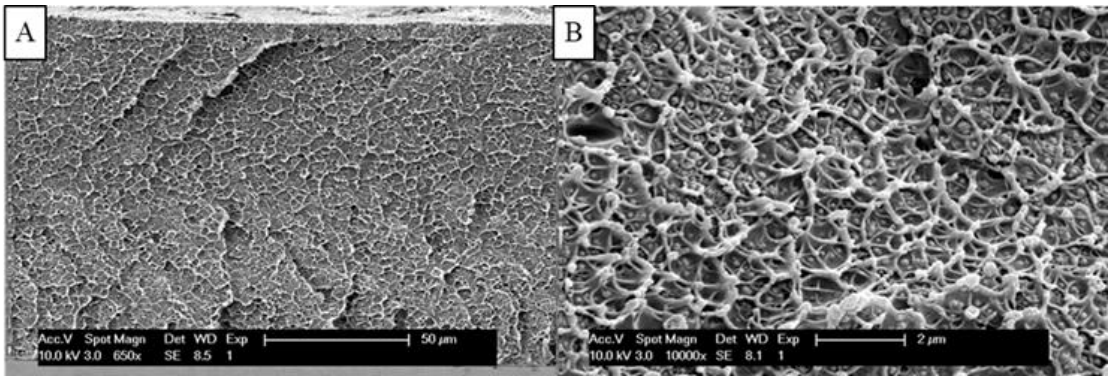

Figure 4: SEM cross-sections of Matrimid-TFA-150. Magnification of 650x (A) and 10000x (B).

Gas permeation experiments

Gas permeation experiments (Figure 5) show that incorporation of MOF-TFA-150 increases the membrane separation factor with 93% from 40 (Matrimid) to 77, while the CO_2 permeability is almost doubled due to incorporation of extra MOF free volume and disruption of the polymer chain packing by the MOFs.[39] Figure 5 clearly shows that the fluorinated MOF reaches higher CO_2/CH_4 separation factors and similar CO_2 permeabilities when compared to AA modulated MOF-808 and UiO-66. Electrostatic dipole-quadrupole interactions between C-F and CO_2 lay at the base of this excellent performance as the C-F bond is intensely polarized due to the large difference in electronegativity between C and F.[40] This results in an increased CO_2 affinity of the fluorinated MOF as confirmed by CO_2 physisorption data (Table 1). Fried et al. reported with help of molecular orbital calculations a maximum quadrupole-dipole interaction energy of -11.5 kJ/mol between CO_2 and $CF_3CH_2CH_3$, situating the quadrupole-dipole interaction strength between London dispersion and hydrogen bonding.[41] Furthermore, it is observed that with decreasing particle size, the MMMs display a small increase in separation factor combined with a minor increase in permeability. The lower separation factor of Matrimid-TFA-1300 can be explained by a less successful incorporation of the large MOF particles in the polymer matrix (as shown by SEM). In contrast with our findings, a constant or a decreasing separation factor with decreasing

ZIF-71 particle size was observed by Japip et al.[42] while a worse performance was found for smaller ZIF-8 particles by Sánchez-Lainez et al. The latter was attributed to a higher degree of clustering when using particles below 150 nm.[43] In our case however, severe particle clustering is largely avoided by using a MMM synthesis method that avoids drying (and thus clustering) of the MOF particles.

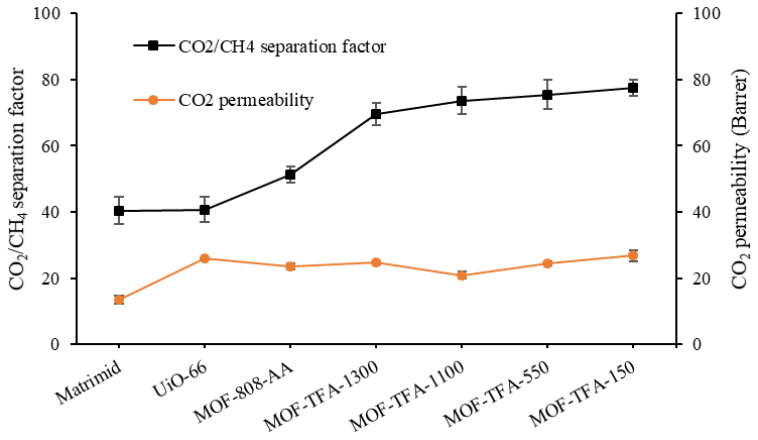

Figure 5: CO_2/CH_4 separation factor and CO_2 permeability of Matrimid and MMMs with different sizes of MOF-TFA. Gas filtrations were performed at 30 °C, 5 bar feed pressure and 50v%/50v% CO_2/CH_4 feed. Lines are added to guide the eye.

When the MOF-TFA loading is increased, no statistical difference in CO_2/CH_4 separation factor can be observed while a substantial increase in CO_2 permeability is observed (Figure 6). Based on the increase in separation factor for 10 wt% MMMs, one could expect a similar improvement for 20 and 30 wt% MMMs. However, gas separation data show that the separation factor only slightly increases for 30 wt% and even slightly decreases for 20 wt%. Nevertheless, due to overlapping standard deviations, the separation factor for all three loadings has to be considered statistically constant, hence suggesting to a certain extent the presence of interfacial defects at higher MOF loading, which would allow unselective gas flow past the MOFs. This could also explain the extremely steep increase in CO_2 permeability for the MMMs with 30 wt% MOF. SEM cross-sections of 20 and 30 wt% MMMs support this hypothesis as particle aggregation can be observed

at higher loadings, resulting in a higher probability of interfacial defects (Figure S9 and 10). Eventually, this results in 30 wt% MMMs with a CO_2 permeability of 63 Barrer at a separation factor of 81. Compared to the pristine Matrimid membrane (with a separation factor of 40 and CO_2 permeability of 14), this means that separation factor is improved with +100% and permeability with +350%.

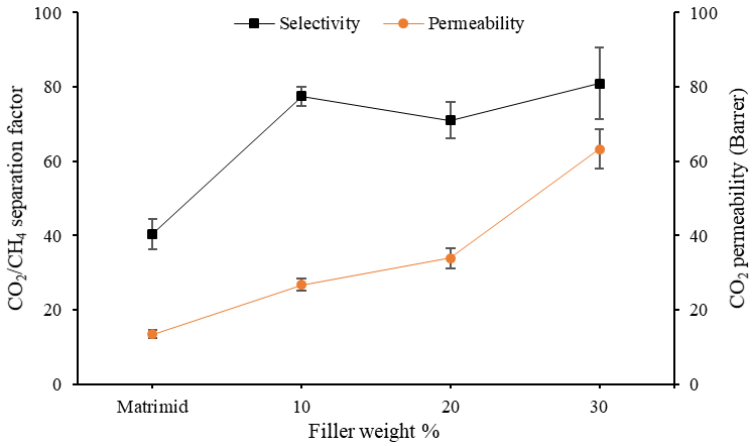

Figure 6: Effect of increasing the loading of MOF-TFA-150. Gas filtrations were performed at 30 °C, 5 bar feed pressure and 50v%/50v% CO_2/CH_4 feed. Lines are added to guide the eye.

Varying the feed pressure (Figure 7) predominantly impacts the CO_2 permeability, whereas CO_2/CH_4 separation factor remains largely unaffected for both the unfilled and the 10 wt% MOF-TFA loaded membrane. By increasing the feed pressure, the permeability of the reference membranes and the MMM steadily drops. This can be considered as typical solution-diffusion behavior since the dual-sorption model predicts a decreased gas solubility in the membrane with increasing pressure and thus, as a consequence, a lowered gas permeability.[44,45] While the separation factor of the MMMs is relatively stable over the entire pressure range (with exception of the MMM separation factor at 10 bar, probably an experimental outlier), the Matrimid membrane loses a substantial part of its separation factor at 15 bar. As the plasticization pressure

of Matrimid is believed to be at around 7-8 bar CO_2 partial pressure[37], this loss in separation factor probably originates from starting plasticization although not yet visible in the permeability result. In addition, the pressure dependency tests show that the MMMs with fluorine functionalized MOF retain their separation factor at elevated feed pressure (which is often not the case for nitrogen or metal based functionalization[46]), thus excluding the possibility of a facilitated transport mechanism.

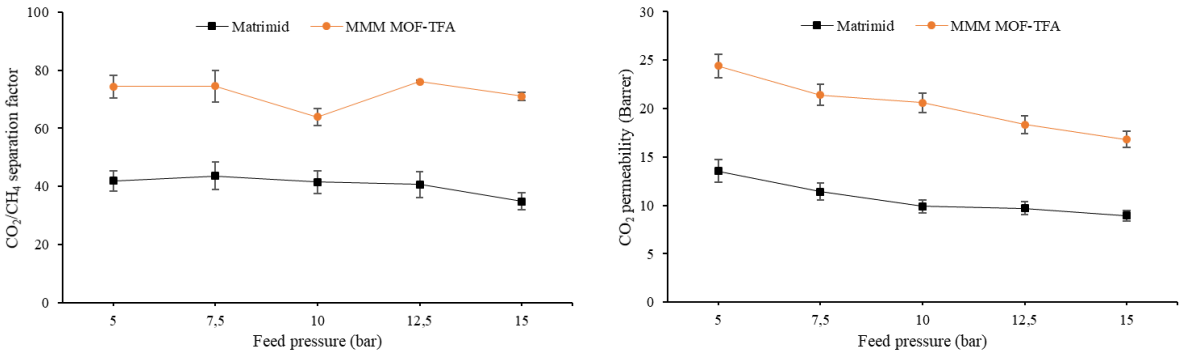

Figure 7: Pressure dependency tests for Matrimid membranes (black, circle) and MMMs with 10 wt% MOF-TFA (orange, square). Gas filtrations were performed at 30 °C and 50v%/50v% CO_2/CH_4 feed. Lines are added to guide the eye.

3.2 Increasing the fluorine concentration inside MOF-808

Characterization of MOFs and membranes

As the incorporation of a fluorinated modulator (TFA) in the first part of this work strongly improved the membrane performance, it was hypothesized that an additional increase in fluorine content might even further enhance the CO_2 separation efficiency of the membrane. Therefore, a series of fluorinated alkyl carboxylic acids were applied as MOF modulators for better CO_2-philicity of the resulting MMMs. Their non-fluorinated analogues were also used as reference materials. A MOF prepared with modulator *x* is simply denoted as MOF-*x*, while the corresponding MMM is named Matrimid-*x* (Table 2).

Table 2: Overview of the MOF and MMM nomenclature used in this section. All MMMs are prepared with 10 wt% MOF loading.

Membrane composition	MOF name	Mixed-matrix membrane name
Matrimid + MOF-808-AA	MOF-AA	Matrimid-AA
Matrimid + MOF-808-PA	MOF-PA	Matrimid-PA
Matrimid + MOF-808-BA	MOF-BA	Matrimid-BA
Matrimid + MOF-808-TFA	MOF-TFA	Matrimid-TFA
Matrimid + MOF-808-PFPA	MOF-PFPA	Matrimid-PFPA
Matrimid + MOF-808-HFBA	MOF-HFBA	Matrimid-HFBA

Figure 8 displays the SEM images and XRD patterns of MOF-808 modulated with AA, PA and BA. All MOFs are highly crystalline and correspond well with the simulated diffractogram of MOF-808. Additionally, SEM images show that the average particle size of the synthesized MOFs decreases with increasing length of the alkyl chain: 850 nm for AA, 650 nm for PA and <100 nm for BA. A decrease in particle size with increasing size of the modulator was also observed by Zhan et al. for their Zr-fumarate MOF.[47]

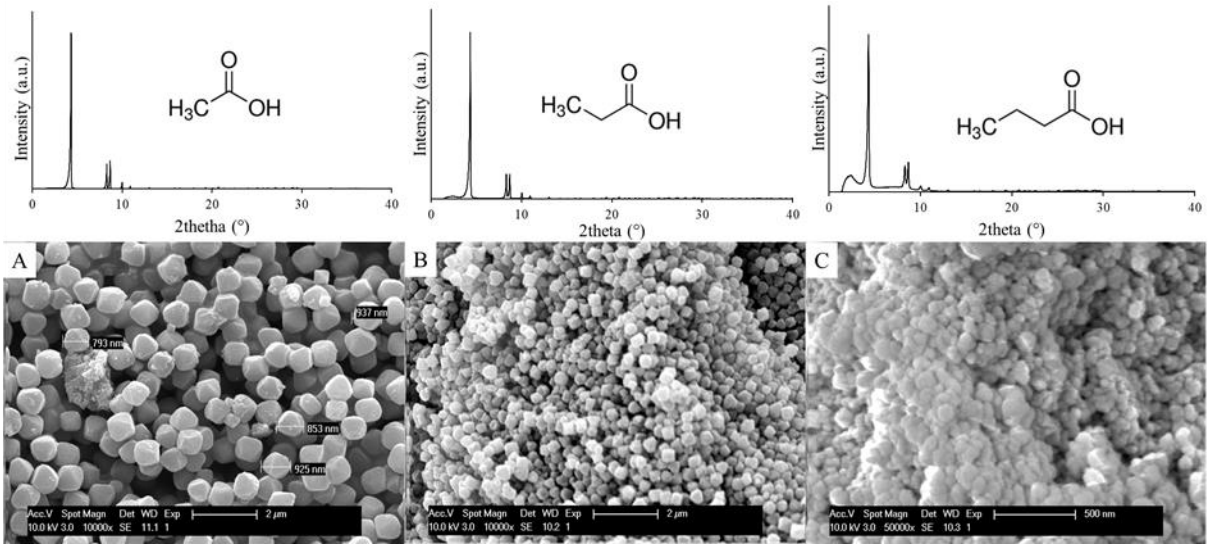

Figure 8: XRD patterns (top) and SEM images (bottom) of (A) MOF-AA, (B) MOF-PA, (C) MOF-BA.

Likewise, XRD and SEM data of the perfluoro-compounds are presented in Figure 9. Whereas the use of TFA and PFPA still results in highly crystalline particles, modulation with HFBA creates a MOF with lower crystallinity. Although the XRD pattern still corresponds with that of MOF-808, significant peak broadening is observed, which is a strong indication for the presence of extremely small particles. Calculations based on the Debye-Scherrer equation indicate a crystallite size of ~15 nm. Therefore, it is hypothesized that the hydrophobic HFBA tails repulse the aqueous synthesis medium during MOF nucleation and growth, preventing connection and further growth of first-stage MOF clusters.

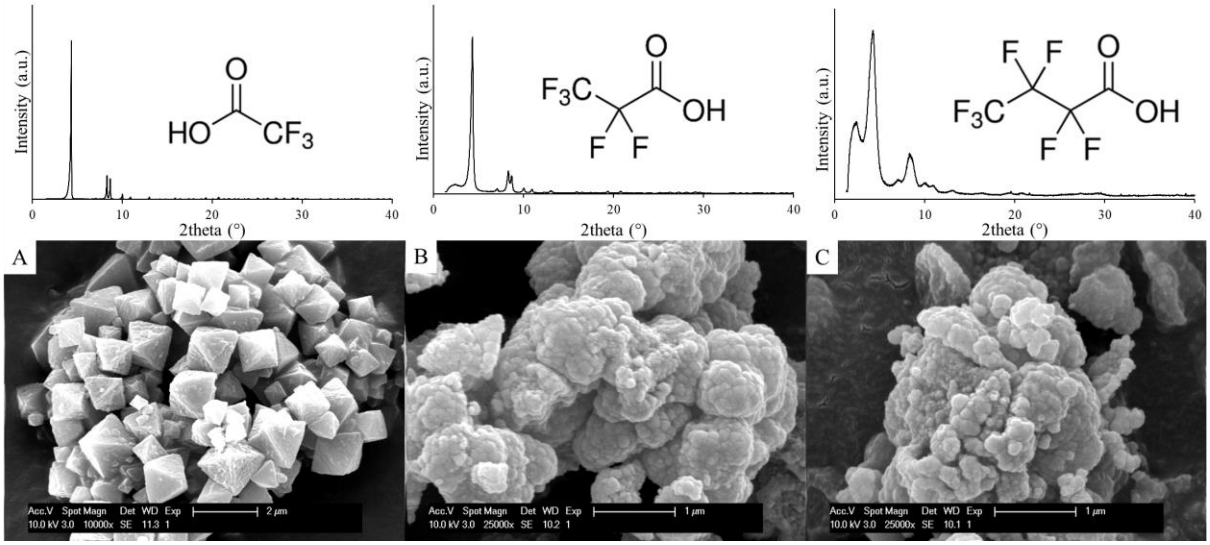

Figure 9: XRD patterns (top) and SEM images (bottom) of (A) MOF-TFA, (B) MOF-PFPA, (C) MOF-HFBA.

NMR shows that AA, PA and BA modulated MOF-808 contained respectively 3.8, 3.2 and 3.9 modulator molecules per Zr-cluster while 4.9 TFA, 4.2 PFPA and 3.9 HFBA molecules were on average incorporated per cluster for the fluorinated MOFs (Table 3). To validate the obtained NMR results, TGA data were taken for MOF-TFA, MOF-PFPA and MOF-HFBA (Figure S34). Thermogravimetric analysis suggests approximatively 4.2, 4.1 and 3.2 molecules of TFA, PFPA and HFBA, respectively, per Zr-cluster and thus confirms the trend obtained by NMR.[48]

IR analysis further confirmed the presence of fluorine groups inside the different MOFs. For TFA, PFPA and HFBA modulated MOF, typical C-F stretching and bending vibrations are seen in Figure S36. Peaks at 1170 cm^{-1} and 1215 cm^{-1} belong respectively to symmetric and asymmetric stretching of -CF_3 groups. -CF_2 stretching becomes visible at 1040 cm^{-1} in the PFPA spectrum. Furthermore, MOF-HFBA shows two extra peaks at 1090 and 1125 cm^{-1}, which Crowder et al. attributed to C-F vibrations of CF_2.[49]

Finally, a decrease in specific surface area of both the non-fluorinated and the fluorinated series with increasing alkyl chain length is observed: 1982 m^2/g (MOF-AA), 1468 m^2/g (MOF-PA) and 739 m^2/g (MOF-BA) for the regular MOFs and 1239 m^2/g (MOF-TFA), 1089 m^2/g (MOF-PFPA) and 622 m^2/g (MOF-HFBA) for the fluorinated MOFs (Figure S37+S38). A similar trend was perceived by Deria et al. when functionalizing NU-1000 using perfluoroalkane ligands with varying chain length.[50] In addition, the MOF pore diameters could be estimated with N_2 physisorption (Figure S39 and S40) and are well in agreement with literature[22]. The small cage with pore diameter of 5-6 Å remains unchanged by varying the modulator while the average pore diameter of the large, adamantine cage gradually decreases with increasing the modulator size for both fluorinated and standard modulators (Table 3). Moreover, CO_2 adsorption experiments prove that MOF-TFA (Figure S17) and MOF-PFPA (Figure S41) have a higher CO_2 affinity than their non-fluorinated counterpart (MOF-AA and MOF-PA, respectively), despite significantly lower BET surface area.

Table 3: BET surface area, pore volume, average pore size, average number of modulator molecules per Zr_6 cluster (as determined by NMR). Glass transition temperature (T_g) of the corresponding 10 wt% Matrimid MMM is given as well. Adsorption isotherms for N_2 and CO_2 are found in SI.

	BET surface area (m^2/g)	**CO_2 uptake (cm^3/g)**	**Pore volume (cm^3/g)**	**Pore size (Å)**	**Modulators per Zr_6 cluster**	**T_g of corresponding MMM (°C)**
MOF-AA	1982	49.8	0.65	18.4	3.8	326
MOF-PA	1468	35.7	0.53	16.7	3.2	325

MOF-BA	739	-	0.27	15.6	3.9	325
MOF-TFA	1239	46.0	0.49	18.4	4.9	326
MOF-PFPA	1089	37.8	0.40	16.7	4.2	324
MOF-HFBA	622	-	0.21	13.8	3.9	324

DSC measurements were performed to determine the T_g of all membranes. Table 3 displays an overall increase in T_g of roughly 10 °C for all MMMs compared to pristine Matrimid, indicating a reduced polymer chain mobility. Table S2 shows that the density of the pristine Matrimid membrane was 1.23 g/cm^3, which is in good agreement with literature[37]. Upon MOF incorporation, density of the MMMs (with exception of Matrimid-HFBA) increased slightly compared to that of pure Matrimid, suggesting a good affinity between MOF and polymer in general[38,51,52]. A notable increase in specific volume was observed for Matrimid-HFBA (Figure S42) compared to the other MMMs. SEM images indicate that TFA and PFPA modulated MOF are well embedded in the polymer matrix (Figure S43) while the SEM cross-sections of Matrimid-HFBA show a non-ideal, irregular MOF incorporation (Figure S44).

Gas permeation experiments

Figure 10 demonstrates that, for the series of MOF modulated with alkyl carboxylic acids, CO_2/CH_4 separation factor was found to be relatively constant with increasing modulator chain length, ranging from 41 (for PA) till 51 (for AA). Both AA and BA MOFs caused a similar increase in permeability of roughly 60%, while PA modulation led to only a minor increase. The use of fluorinated MOFs boosts the MMM performance (both separation factor and CO_2 permeability) with an optimal separation factor of 97 observed for MOF-PFPA combined with a CO_2 permeability of 29 Barrer. CO_2 physisorption data demonstrated that the fluorinated modulator improved the CO_2 affinity of the MOF (Table 1 and Table 3). Furthermore, N_2 physisorption shows that the pore size gradually decreases with increasing modulator chain length. For HFBA and BA

modulated MOF, the pore size still remains 13.8 and 15.8 Å respectively, which largely excludes the possibility of size sieving by the MOF, considering the kinetic diameters of CO_2 (3.3 Å) and CH_4 (3.8 Å)[53]. Additionally, DSC reveals an increased T_g for all MMMs and thus a certain degree of polymer rigidification at the polymer-particle interface (Table 3). This may contribute to an enhanced separation factor but a similar degree of polymer rigidification should be assumed for incorporation of all MOFs as no notable differences in T_g were observed between the individual samples. A substantial decrease in separation factor is observed when MOF-HFBA is used, possibly caused by interfacial defects (as suggested by SEM and density measurements) which may arise from low compatibility between the highly fluorinated MOF and the non-fluorinated polymer. The strongly increased permeability (higher than expected) for Matrimid-HFBA further adds to this hypothesis of existing molecular voids between polymer and filler. This is also visible in Figure S45, which shows the change in membrane morphology and structure upon incorporation of HFBA modulated MOF.

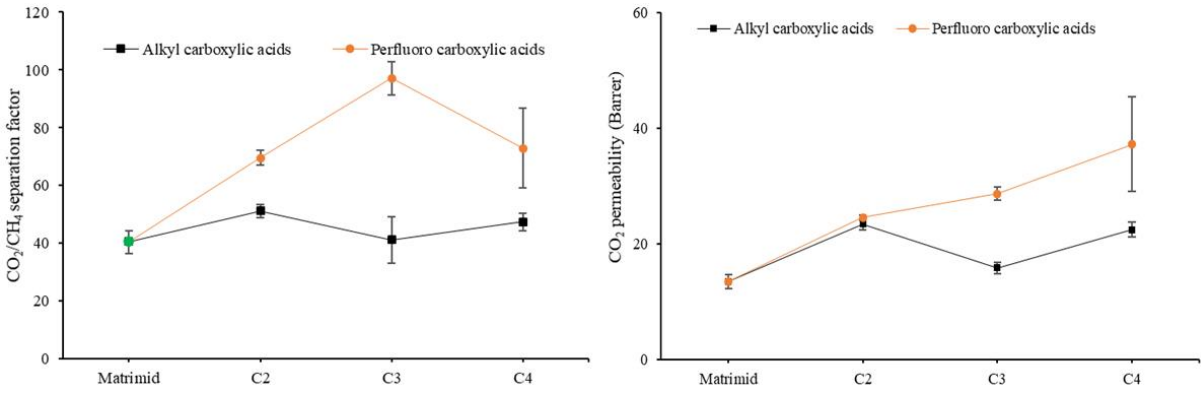

Figure 10: Left: CO_2/CH_4 separation factor comparison between MMMs made with MOF modulated by alkyl carboxylic acids (black, square) and by perfluoro carboxylic acids (orange, circles). Right: CO_2 permeability of Matrimid and MMMs. Gas filtrations were performed at 30 °C, 5 bar feed pressure and 50v%/50v% CO_2/CH_4 feed. Lines are added to guide the eye.

3.3 Comparison with literature

In Figure 11 and Table S3, the MMMs obtained in this study are compared to literature and the upper bounds determined by Robeson in 2008[2] and by Wang in 2018[54]. All MMMs containing MOFs modulated by fluorinated carboxylic acids cross the mixed-gas upper bound, while MMMs based on MOF-AA, MOF-PA and MOF-BA all fall under this limit. The 30 wt% Matrimid-TFA and 10 wt% Matrimid-PFPA MMMs even cross the 2008 Robeson upper bound with their performance. This is especially remarkable when considering that the starting material, Matrimid, is only a moderately performing polymer with a separation factor-permeability combination far below both upper bounds. When comparing to literature (Table S3), it can be concluded that MMMs based on regular MOF-808 show similar or improved performance compared to UiO-66 based MMMs, while Matrimid MMMs with fluorinated MOF-808 clearly outperform these UiO-66 MMMs and belong to the best performing Zr-based MOF MMMs reported so far.

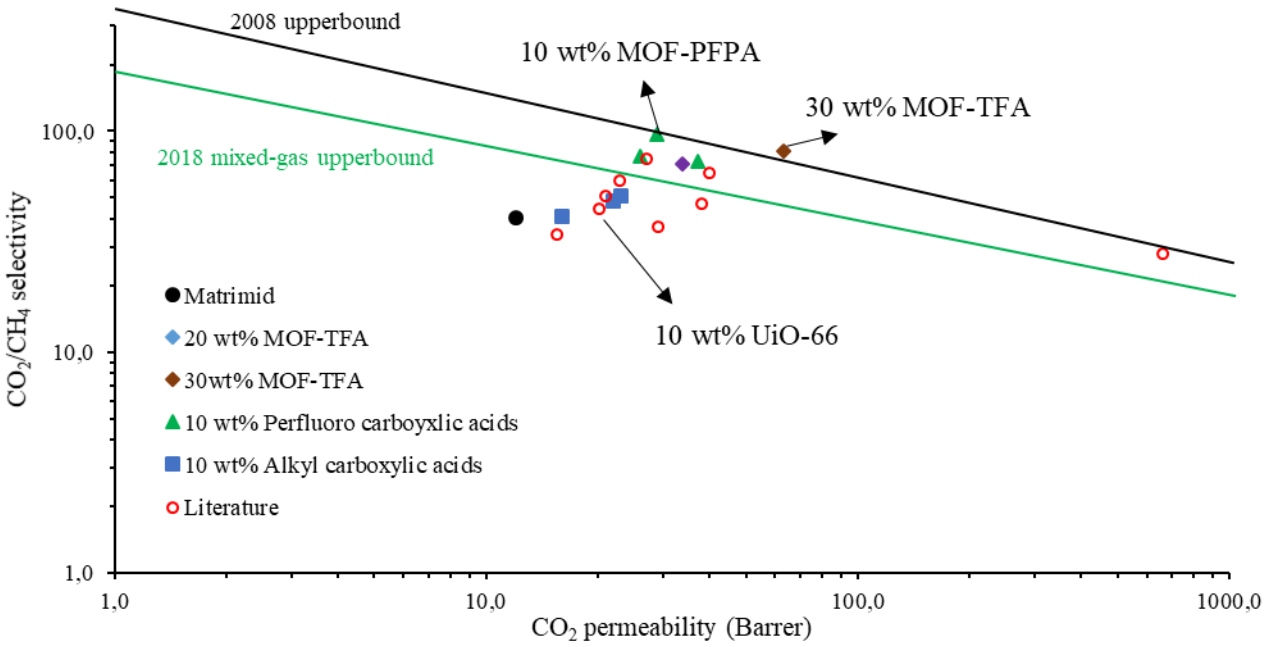

Figure 11: Comparison of prepared MMMs with literature in a selectivity-permeability plot.

4 Conclusions

MOF-808 holds promise as a highly versatile MOF for CO_2 capture due to its low preparation cost, excellent intrinsic features (stability, porosity, specific surface) and, most importantly, simple functionalization. MOF-808 can be very easily tuned in terms of particle morphology and inner and outer surface functionalities by playing with MOF synthesis parameters and (cheap) modulator types. Furthermore, the MOF can be prepared in water, excluding the use of toxic organic solvents (e.g. DMF) traditionally used in MOF synthesis. "Modulator Mediated Functionalization" (MoFu) is a novel and straightforward tool to tune the separation potential of MOFs, exemplified here for the CO_2-philicity of MOF-808. The obtained CO_2 separation performance of the prepared MOF-808 MMMs was outstanding. Two of the best MMMs prepared with 30 wt% MOF-TFA and 10 wt% MOF-PFPA improved the CO_2/CH_4 separation factor with 100% and 140%, respectively. At the same time, both MOFs significantly enhanced the CO_2 permeability (+350% and +100%). As a result, Matrimid-TFA-30 and Matrimid-PFPA crossed the 2008 and 2018 performance upper bounds. When considering that Matrimid, a medium performance polymer, was used as starting material, the prepared MMMs rank among the best in both absolute and relative performance increase so far found in literature. Although here demonstrated for CO_2/CH_4 separation, the presented MoFu-concept is in theory applicable to all separation domains (both gas and liquid) that involve MOF-based membranes.

Associated content

Supporting Information

Simulated XRD spectrum of MOF-808; XRD spectra of all synthesized MOFs; SEM cross-sections of Matrimid membrane and MMMs with 10, 20, 30 wt% MOF-TFA, MMMs with 10 wt% MOF-AA, MOF-PA, MOF-BA, MOF-PFPA, MOF-HFBA; Size distribution plot of MOF-TFA-150, MOF-TFA-550 and MOF-TFA-1300 based on ImageJ analysis; ATR-FTIR spectra of all synthesized MOFs and membranes; N_2 and CO_2 adsorption isotherms of MOF-AA, MOF-TFA, MOF-PA and MOF-PFPA; Plots of cumulative

pore volume and incremental pore volume as a function of pore width for MOF-AA, MOF-PA, MOF-BA, MOF-TFA, MOF-PFPA and MOF-HFBA; TGA analysis of Matrimid membrane and MMMs with 10 wt% MOF-TFA-150, MOF-TFA-550, MOF-TFA-1300; NMR analysis of MOF-AA, MOF-PA, MOF-BA, MOF-TFA, MOF-PFPA, MOF-HFBA; DSC spectra of MMMs with 10 wt% MOF-AA, MOF-PA, MOF-BA, MOF-TFA, MOF-PFPA and MOF-HFBA; Density value for all membranes; Photographic pictures of membrane coupons of Matrimid and MMMs with 10 wt% MOF-TFA, MOF-PFPA and MOF-HFBA; Table overview of similar MMMs reported in literature.

Author information

Corresponding author

*E-mail: ivo.vankelecom@kuleuven.be

Tel: +32 16 32 15 94

Conflicts of interest

There are no conflicts to declare.

Acknowledgements

R.T. and N.V.V. are grateful to the FWO for their SB-PhD fellowships (1S63317N and 1S32917N). S.S. thanks FWO for funding through an Aspirant grant (1104118N). The authors would like to thank Kristien van der Flaas for help with the DSC measurements.

References

(1) Sanders, D. F.; Smith, Z. P.; Guo, R.; Robeson, L. M.; McGrath, J. E.; Paul, D. R.; Freeman, B. D. Energy-Efficient Polymeric Gas Separation Membranes for a Sustainable Future: A Review. Polymer (Guildf). 2013, 54 (18), 4729–4761. https://doi.org/10.1016/j.polymer.2013.05.075.

(2) Robeson, L. M. The Upper Bound Revisited. J. Memb. Sci. 2008, 320 (1–2), 390–400. https://doi.org/10.1016/j.memsci.2008.04.030.

(3) Basu, S.; Khan, A. L.; Cano-Odena, A.; Liu, C.; Vankelecom, I. F. J. Membrane-Based Technologies for Biogas Separations. Chem. Soc. Rev. 2010, 39 (2), 750–768. https://doi.org/10.1039/B817050A.

(4) Katayama, Y.; Bentz, K. C.; Cohen, S. M. Defect-Free MOF-Based Mixed-Matrix Membranes Obtained by Corona Cross-Linking. ACS Appl. Mater. Interfaces 2019, 11, 13029–13037. https://doi.org/10.1021/acsami.9b02539.

(5) Marti, A. M.; Venna, S. R.; Roth, E. A.; Culp, T.; Hopkinson, D. P. Simple Fabrication Method for Mixed Matrix Membranes with in Situ MOF Growth for Gas Separation. ACS Appl. Mater. Interfaces 2018, 10, 24784–24790. https://doi.org/10.1021/acsami.8b06592.

(6) Liu, G.; Labreche, Y.; Chernikova, V.; Shekhah, O.; Zhang, C.; Belmabkhout, Y.; Eddaoudi, M.; Koros, W. J. Zeolite-like MOF Nanocrystals Incorporated 6FDA-Polyimide Mixed-Matrix Membranes for CO2/CH4 Separation. J. Memb. Sci. 2018, 565 (August), 186–193. https://doi.org/10.1016/j.memsci.2018.08.031.

(7) Qian, Q.; Wu, A. X.; Chi, W. S.; Asinger, P. A.; Lin, S.; Hypsher, A.; Smith, Z. P. Mixed-Matrix Membranes Formed from Imide-Functionalized UiO-66-NH2 for Improved Interfacial Compatibility. ACS Appl. Mater. Interfaces 2019, 11, 31257–31269. https://doi.org/10.1021/acsami.9b07500.

(8) Kertik, A.; Wee, L. H.; Pfannmoeller, M.; Bals, S.; Martens, J.; Vankelecom, I. F. J. Highly Selective Gas Separation Membrane Using In-Situ Amorphised Metal-Organic Frameworks. Energy Environ. Sci. 2017, 10, 2342–2351. https://doi.org/10.1039/C7EE01872J.

(9) Zhang, Y.; Musselman, I. H.; Ferraris, J. P.; Balkus Jr, K. J. Gas Permeability Properties of Matrimid Membranes Containing the Metal-Organic Framework Cu–BPY–HFS. J. Memb. Sci. 2008, 313, 170–181. https://doi.org/10.1016/j.memsci.2008.01.005.

(10) Perez, E. V; Balkus Jr, K. J.; Ferraris, J. P.; Musselman, I. H. Mixed-Matrix Membranes Containing MOF-5 for Gas Separations. J. Memb. Sci. 2009, 328, 165–173. https://doi.org/10.1016/j.memsci.2008.12.006.

(11) Ma, C.; Urban, J. J. Enhanced CO2 Capture and Hydrogen Purification by Hydroxy Metal–Organic Framework/Polyimide Mixed Matrix Membranes. ChemSusChem 2019, 12, 1–8. https://doi.org/10.1002/cssc.201902248.

(12) Marti, A. M.; Venna, S. R.; Roth, E. A.; Culp, J. T.; Hopkinson, D. P. Simple Fabrication Method for Mixed Matrix Membranes with in Situ MOF Growth for Gas Separation. ACS Appl. Mater. Interfaces 2018, 10, 24787–24790. https://doi.org/10.1021/acsami.8b06592.

(13) Prasetya, N.; Donose, B. C.; Ladewig, B. P. A New and Highly Robust Light-Responsive Azo-UiO-66 for Highly Selective and Low Energy Post-Combustion CO2 Capture and Its Application in a Mixed-Matrix Membrane for CO2/N2 Separation. J. Mater. Chem. A 2018, 6, 16390–16402. https://doi.org/10.1039/c8ta03553a.

(14) Sutrisna, P.; Hou, J.; Zulkifli, M.; Li, H.; Zhang, Y.; Liang, W.; D'Alesandro, D.; Chen, V. Surface Functionalized UiO-66/Pebax-Based Ultrathin Composite Hollow Fiber Gas Separation Membranes. J. Mater. Chem. A 2018, 6, 918–931. https://doi.org/10.1039/C7TA07512J.

(15) Ahmad, M. Z.; Navarro, M.; Lhotka, M.; Zornoza, B.; Téllez, C.; Vos, W. M. De; Benes, N. E.; Konnertz, N. M.; Visser, T.; Semino, R.; Maurin, G.; Fila, V.; Coronas, J. Enhanced Gas Separation Performance of 6FDA-DAM Based Mixed Matrix Membranes by Incorporating MOF UiO-66 and Its Derivatives. J. Memb. Sci. 2018, 558 (March), 64–77. https://doi.org/10.1016/j.memsci.2018.04.040.

(16) Seoane, B.; Coronas, J.; Gascon, I.; Benavides, M. E.; Karvan, O.; Caro, J.; Kapteijn, F.; Gascon, J. Metal – Organic Framework Based Mixed Matrix Membranes: A Solution for Highly Efficient CO2 Capture? Chem. Soc. Rev. 2015, 44, 2421–2454. https://doi.org/10.1039/C4CS00437J.

(17) Anjum, M. W.; Vermoortele, F.; Khan, A. L.; Bueken, B.; Vos, D. E. De; Vankelecom, I. F. J. Modulated UiO-66-Based Mixed-Matrix Membranes for CO2 Separation. ACS Appl. Mater. Interfaces 2015, 7, 25193–25201. https://doi.org/10.1021/acsami.5b08964.

(18) Cavka, J. H.; Jakobsen, S.; Olsbye, U.; Guillou, N.; Lamberti, C.; Bordiga, S.; Lillerud, K. P. A New Zirconium Inorganic Building Brick Forming Metal Organic Frameworks with Exceptional Stability. J. Am. Chem. Soc. Commun. 2008, 130, 13850–13851.

(19) Li, H.; Eddaoudi, M.; O'Keeffe, M.; Yaghi, O. M. Design and Synthesis of an Exceptionally Stable and Highly Porous Metal-Organic Framework. Nature 1999, 402 (November), 276–279.

(20) Mautschke, H.; Drache, F.; Senkovska, I.; Kaskel, S.; Llabrés i Xamena, F. X. Catalytic Properties of Pristine and Defect-Engineered Zr-MOF-808 Metal Organic Frameworks. Catal. Sci. Technol. 2018, 8 (14), 3610–3616. https://doi.org/10.1039/c8cy00742j.

(21) Thür, R.; Van Velthoven, N.; Slootmaekers, S.; Didden, J.; Verbeke, R.; Smolders, S.; Egger, W.; Dickmann, M.; De Vos, D.; Vankelecom, I. F. J. Bipyridine-Based UiO-67 as Novel Filler in Mixed-Matrix Membranes for CO2-Selective Gas Separation. J. Memb. Sci. 2019, 576 (15 April 2019), 78–87. https://doi.org/10.1016/j.memsci.2019.01.016.

(22) Furukawa, H.; Gándara, F.; Zhang, Y.-B.; Jiang, J.; Queen, W. L.; Hudson, M. R.; Yaghi, O. M. Water Adsorption in Porous Metal−Organic Frameworks and Related Materials. J. Am. Chem. Soc. 2014, 136, 4369–4381. https://doi.org/10.1021/ja500330a.

(23) Van Velthoven, N.; Waitschat, S.; Chavan, S. M.; Liu, P.; Smolders, S.; Vercammen, J.; Bueken, B.; Bals, S.; Lillerud, K. P.; Stock, N.; De Vos, D. Single-Site Metal–Organic Framework Catalysts for the Oxidative Coupling of Arenes via C–H/C–H Activation. Chem. Sci. 2019. https://doi.org/10.1039/c8sc05510f.

(24) Jiang, J.; Gándara, F.; Zhang, Y.-B.; Na, K.; Yaghi, O. M.; Klemperer, W. G. Superacidity in Sulfated Metal − Organic Framework-808. J. Am. Chem. Soc. 2014, 136, 12844–12847. https://doi.org/10.1021/ja507119n.

(25) Jia, C.; Cirujano, F. G.; Bueken, B.; Claes, B.; Jonckheere, D.; Van Geem, K. M.; De Vos, D. Geminal Coordinatively Unsaturated Sites on MOF-808 for the Selective Uptake of

Phenolics from a Real Bio-Oil Mixture. ChemSusChem 2019, 101, 1256–1266. https://doi.org/10.1002/cssc.201802692.

(26) Zheng, H.-Q.; Liu, C.-Y.; Zeng, X.-Y.; Chen, J.; Lu, J.; Lin, R.-G.; Cao, R.; Lin, Z.; Su, J. MOF-808: A Metal−Organic Framework with Intrinsic Peroxidase-Like Catalytic Activity at Neutral PH for Colorimetric Biosensing. Inorg. Chem. 2018, 57, 9096–9104. https://doi.org/10.1021/acs.inorgchem.8b01097.

(27) Howarth, A. J.; Liu, Y.; Li, P.; Li, Z.; Wang, T. C.; Hupp, J.; Farha, O. K. Chemical, Thermal and Mechanical Stabilities of Metal-Organic Frameworks. Nat. Rev. | Mater. 2016, No. 15018, 1–15. https://doi.org/10.1038/natrevmats.2015.18.

(28) Reinsch, H.; Waitschat, S.; Chavan, S. M.; Lillerud, K. P.; Stock, N. A Facile "Green" Route for Scalable Batch Production and Continuous Synthesis of Zirconium MOFs. Eur. J. Inorg. Chem. 2016, 2016 (27), 4490–4498. https://doi.org/10.1002/ejic.201600295.

(29) Kertik, A.; Khan, A. L.; Vankelecom, I. F. J. Mixed Matrix Membranes Prepared from Non-Dried MOFs for CO2/CH4 Separations. RSC Adv. 2016, 6, 114505–114512. https://doi.org/10.1039/c6ra23013j.

(30) Rouquerol, F.; Rouquerol, J.; Sing, K. Adsorption by Powders and Porous Solids, 11th ed.; Academic Press: San Diego, 1999.

(31) Walton, K. S.; Snurr, R. Q. Applicability of the BET Method for Determining Surface Areas of Microporous Metal-Organic Frameworks. J. Am. Chem. Soc. 2007, 129 (27), 8552–8556. https://doi.org/10.1021/ja071174k.

(32) Didden, J.; Thür, R.; Volodin, A.; Vankelecom, I. F. J. Blending PPO-Based Molecules with Pebax MH 1657 in Membranes for Gas Separation. J. Appl. Polym. Sci. 2018, 135, 46433. https://doi.org/10.1002/app.46433.

(33) Khan, A. L.; Basu, S.; Cano-odena, A.; Vankelecom, I. F. J. Novel High Throughput Equipment for Membrane-Based Gas Separations. J. Memb. Sci. 2010, 354 (1–2), 32–39. https://doi.org/10.1016/j.memsci.2010.02.069.

(34) Beg, M. A. A.; Clark, H. C. Chemistry of the Trifluoromethyl Group: PART V. Infrared Spectra of Some Phosphorus Compounds Containing CF3. Can. J. Chem. 1962, 40 (3), 393–398. https://doi.org/https://doi.org/10.1139/v62-063.

(35) Bueken, B.; Van Velthoven, N.; Willhammar, T.; Stassin, T.; Stassen, I.; Keen, D. A.; Baron, G. V; Denayer, J. F. M.; Ameloot, R.; Bals, S.; De Vos, D.; Bennett, T. Gel-Based Morphological Design of Zirconium Metal-Organic Frameworks. Chem. Sci. 2017, 8, 3939–3948. https://doi.org/10.1039/c6sc05602d.

(36) Yoreo, J. J. De; Vekilov, P. G. Principles of Crystal Nucleation and Growth. Rev. Mineral. Geochemistry 2003, 54 (1), 57–93. https://doi.org/https://doi.org/10.2113/0540057.

(37) Shahid, S.; Nijmeijer, K. High Pressure Gas Separation Performance of Mixed-Matrix Polymer Membranes Containing Mesoporous Fe(BTC). J. Memb. Sci. 2014, 459, 33–44. https://doi.org/10.1016/j.memsci.2014.02.009.

(38) Zhang, Y.; Balkus Jr, K. J.; Musselman, I. H.; Ferraris, J. P. Mixed-Matrix Membranes Composed of Matrimid® and Mesoporous ZSM-5 Nanoparticles. J. Memb. Sci. 2008, 325, 28–39. https://doi.org/10.1016/j.memsci.2008.04.063.

(39) Etxeberria-Benavides, M.; David, O.; Johnson, T.; Magdalena, M. Ł.; Orsi, A.; Wright, P. A.; Mastel, S.; Hillenbrand, R.; Kapteijn, F.; Gascon, J. High Performance Mixed Matrix Membranes (MMMs) Composed of ZIF-94 Filler and 6FDA-DAM Polymer. 2018, 550 (August 2017), 198–207. https://doi.org/10.1016/j.memsci.2017.12.033.

(40) Cece, A.; Jureller, S. H.; Kerschner, J. L.; Moschner, K. F. Molecular Modeling Approach for Contrasting the Interaction of Ethane and Hexafluoroethane with Carbon Dioxide. J. Phys. Chem. 1996, 3654 (95), 7435–7439. https://doi.org/10.1021/jp953627q.

(41) Fried, J. R.; Hu, N. The Molecular Basis of CO2 Interaction with Polymers Containing Fluorinated Groups: Computational Chemistry of Model Compounds and Molecular Simulation of Poly[Bis(2,2,2-Trifluoroethoxy)Phosphazene]. Polymer (Guildf). 2003, 44, 4363–4372. https://doi.org/10.1016/S0032-3861(03)00285-4.

(42) Japip, S.; Wang, H.; Xiao, Y.; Chung, T. S. Highly Permeable Zeolitic Imidazolate Framework (ZIF)-71 Nano-Particles Enhanced Polyimide Membranes for Gas Separation. J. Memb. Sci. 2014, 467, 162–174. https://doi.org/10.1016/j.memsci.2014.05.025.

(43) Sánchez-Laínez, J.; Zornoza, B.; Friebe, S.; Caro, J.; Cao, S.; Sabetghadam, A.; Seoane, B.; Gascon, J.; Kapteijn, F.; Le Guillouzer, C.; Clet, G.; Daturi, M.; Téllez C.; Coronas, J. Influence of ZIF-8 Particle Size in the Performance of Polybenzimidazole Mixed Matrix Membranes for Pre-Combustion CO2 Capture and Its Validation through Interlaboratory Test. J. Memb. Sci. 2016, 515, 45–53. https://doi.org/10.1016/j.memsci.2016.05.039.

(44) Matteucci, S.; Yampolskii, Y.; Freeman, B. D.; Pinnau, I. Transport of Gases and Vapors in Glassy and Rubbery Polymers. In Materials Science of Membranes for Gas and Vapor Separation; 2006; pp 1–48.

(45) Paul, D. R. Gas Sorption and Transport in Glassy Polymers. Berichte der Bunsengesellschaft für Phys. Chemie 1979, 83 (4), 294–302. https://doi.org/https://doi.org/10.1002/bbpc.19790830403.

(46) Li, Y.; Wang, S.; He, G.; Wu, H.; Pan, F.; Jiang, Z. Facilitated Transport of Small Molecules and Ions for Energy-Efficient Membranes. Chem. Soc. Rev. 2015, 44, 103–118. https://doi.org/10.1039/c4cs00215f.

(47) Zahn, G.; Albert, H.; Lippke, J.; König, S.; Sazama, U.; Fröba, M.; Behrens, P. A Water-Born Zr-Based Porous Coordination Polymer: Modulated Synthesis of Zr-Fumarate MOF. Microporous Mesoporous Mater. 2015, 203, 186–194. https://doi.org/10.1016/j.micromeso.2014.10.034.

(48) Bueken, B.; Van Velthoven, N.; Krajnc, A.; Smolders, S.; Taulelle, F.; Mellot-Draznieks, C.; Mali, G.; Bennett, T. D.; De Vos, D. Tackling the Defect Conundrum in UiO-66: A Mixed-Linker Approach to Engineering Missing Linker Defects. Chem. Mater. 2017, 29 (24), 10478–10486. https://doi.org/10.1021/acs.chemmater.7b04128.

(49) Crowder, G. A. Infrared Spectra of Heptafluorbutyric Acid and Some of Its Esters. J. Fluor. Chem. 1973, 3 (2), 133–140. https://doi.org/https://doi.org/10.1016/S0022-1139(00)84158-5.

(50) Deria, P.; Mondloch, J. E.; Tylianakis, E.; Ghosh, P.; Bury, W.; Snurr, R. Q.; Hupp, J. T.; Farha, O. K. Perfluoroalkane Functionalization of NU-1000 via Solvent-Assisted Ligand Incorporation: Synthesis and CO2 Adsorption Studies. J. Am. Chem. Soc. 2013, 14, 16801–16804. https://doi.org/10.1021/ja408959g.

(51) Shahid, S.; Nijmeijer, K. Performance and Plasticization Behavior of Polymer – MOF Membranes for Gas Separation at Elevated Pressures. J. Memb. Sci. 2014, 470, 166–177. https://doi.org/10.1016/j.memsci.2014.07.034.

(52) Ren, H.; Jin, J.; Hu, J.; Liu, H. Affinity between Metal − Organic Frameworks and Polyimides in Asymmetric Mixed Matrix Membranes for Gas Separations. Ind. Eng. Chem. Res. 2012, 51, 10156–10164. https://doi.org/10.1021/ie300553k.

(53) Baker, R. W.; Lokhandwala, K. Natural Gas Processing with Membranes: An Overview. Ind. Eng. Chem. Res. 2008, 47, 2109–2121.

(54) Wang, Y.; Ma, X.; Ghanem, B. S.; Alghunaimi, F.; Pinnau, I.; Han, Y. Polymers of Intrinsic Microporosity for Energy-Intensive Membrane-Based Gas Separations. Mater. Today Nano 2019, 3 (2018), 69–95. https://doi.org/10.1016/j.mtnano.2018.11.003.

(55) Castarlenas, S.; Téllez, C.; Coronas, J. Gas Separation with Mixed Matrix Membranes Obtained from MOF UiO-66- Graphite Oxide Hybrids. J. Memb. Sci. 2017, 526, 205–211. https://doi.org/10.1016/j.memsci.2016.12.041.

(56) Sabetghadam, A.; Seoane, B.; Keskin, D.; Duim, N.; Rodenas, T.; Shahid, S.; Sorribas, S.; Guillouzer, C. Le; Clet, G.; Tellez, C.; Daturi, M.; Coronas, J.; Kapteijn, F.; Gascon, J. Metal Organic Framework Crystals in Mixed-Matrix Membranes: Impact of the Filler Morphology on the Gas Separation Performance. Adv. Funct. Mater. 2016, 26, 3154–3163. https://doi.org/10.1002/adfm.201505352.

(57) Carter, D.; Tezel, F. H.; Kruczek, B.; Kalipcilar, H. Investigation and Comparison of Mixed Matrix Membranes Composed of Polyimide Matrimid with ZIF–8 , Silicalite , and SAPO–34. J. Memb. Sci. 2017, 544 (May), 35–46. https://doi.org/10.1016/j.memsci.2017.08.068.

(58) Venna, S. R.; Lartey, M.; Li, T.; Spore, A.; Kumar, S.; Nulwala, H. B.; Luebke, D. R.; Rosi, L.; Albenze, E. Fabrication of MMMs with Improved Gas Separation Properties Using Externally-Functionalized MOF Particles. J. Mater. Chem. A 2015, 3, 5014–5022. https://doi.org/10.1039/c4ta05225k.

(59) Jiang, Y.; Liu, C.; Caro, J.; Huang, A. A New UiO-66-NH2 Based Mixed-Matrix Membranes with High CO2/CH4 Separation Performance. Microporous Mesoporous Mater. 2019, 274 (July 2018), 203–211. https://doi.org/10.1016/j.micromeso.2018.08.003.